Measurement 152 (2020) 107345

Contents lists available at ScienceDirect

Measurement

journal homepage: www.elsevier.com/locate/measurement

Multi-sensor network for industrial metal plate structure monitoring via time reversal ultrasonic guided wave

Zhang Hanfei [a,b,*], Cao Shuhao [a], Ma Shiwei [a,*], Lu Yu [a], Xiong Hanyu [a], Xia Qingwei [a], Liu Yanyan [a], Zhang Haiyan [c]

[a] School of Mechatronic Engineering and Automation, Shanghai University, Shanghai, China
[b] Information Service and Information Research Center, Huaiyin Normal University, Jiangsu, China
[c] School of Communication and Information Engineering, Shanghai University, Shanghai, China

ARTICLE INFO

Article history:
Received 1 July 2019
Received in revised form 17 November 2019
Accepted 29 November 2019
Available online 2 December 2019

Keywords:
Lamb wave
Damage localization
Baseline-free
Time reversal

ABSTRACT

Active ultrasonic guided wave is considered to be the most effective and important on-line damage monitoring method for industrial steel plates structure health monitoring. Aiming at the problem of poor practicability of extracting damage scattering signal from baseline signal, a baseline-free time reversal probabilistic imaging algorithm (BFTRPI algorithm) is proposed in this paper based on ultrasound guided waves time reversal theory and probability statistics principle. Firstly, the time reversal of signal and the adaptive focusing mechanism of wave source are used to eliminate the dispersion effect of Lamb wave by the multi-sensor network. Secondly, the energy characteristic difference coefficient between the reconstructed Lamb wave signal and the original excitation signal, is taken as the damage factor. Finally, the relative distance between the damage and the direct path of the sensor-actuator channel is used to adjust the weight distribution function. The weighted probabilistic values of each sensor path in the sensor network are mapped to the discrete coordinates in the detection area, and the probabilistic imaging of the damage appearing on these discrete coordinates is constructed for multiple damages imaging and location. Experiments on aluminium sheets show that the method can clearly separate the damage scattering signals without baseline signals, achieve the focus of the original excitation signal, and obtain the damage probability images of structure. Compared to traditional probability distribution function method, it has better imaging accuracy and imaging quality. The positioning accuracy of the BFTRPI algorithm is obviously higher than that of traditional algorithm. The estimated position by BFTRPI algorithm is more close to the actual damage position. The location area of damage and artifact for traditional algorithm are both higher than that of BFTRPI algorithm. This method can accurately identify and locate multiple damages in aluminium sheet, which verifies the validity of this method and has certain engineering application value.

1. Introduction

Plate metal structures are widely used in various industrial fields, such as the fuselage of fixed-wing aircraft, wings and hatches, the fuselage and propeller blades of rotary-wing aircraft, hulls of ships and submarines, tanks of liquid rocket fuels, etc. Corrosion and cracks are the main damage forms of such structures. In the process of production and service, plate metals are affected by certain external factors (load, temperature change and corrosive medium) and internal factors (vibration transmitted by rotating parts), and the structure will gradually aging. The main manifestation of plate metals is that different degrees of damage occur, resulting in the decrease of the bearing capacity of the structure. As the most common guided waves in ultrasonic nondestructive testing, Lamb wave has the characteristics of small attenuation along the propagation path and long propagation distance, which is also sensitive to minor damage and has great advantages in large area nondestructive examination of plate structures [1,2]. Ultrasound guided waves have been used for nondestructive testing of immersive water structures, such as hulls, submarines and underwater pipelines [3,4]. The main tasks of structural health monitoring are to determine whether there is damage, locate the damage, evaluate the type and extent of damage, analyze and predict structural life and evaluate structural safety. The damage location is an important part of structural health monitoring [5-9].

* Corresponding author at: School of Mechatronic Engineering and Automation, Shanghai University, Shanghai, China.
E-mail addresses: zhanghanfei2006@163.com (Z. Hanfei), masw@shu.edu.cn (M. Shiwei).

https://doi.org/10.1016/j.measurement.2019.107345
0263-2241/

For the Lamb wave damage location, researchers have carried out a lot of research [10-12]. Traditional damage location methods based on the propagation time of damage scattering signal, such as array composite imaging, probabilistic damage imaging, sparse imaging [10,13,14]. In the active Lamb wave structural health monitoring, the scattering signal caused by damage is often weak and easily submerged by direct wave, reflected wave from boundary and signals caused by mode conversion in the process of Lamb wave propagation. Most active Lamb wave damage monitoring methods use the baseline signal to obtain the damage scattering signal. By taking the health signal as the baseline signal, the damage scattering signal is the difference between the structural response signal under the damage state and the baseline signal. But in practical application, this method is vulnerable to the influence of environmental temperature, structural boundary, stress condition, external vibration, and artificial operation error. And damage scattering signal is easily submerged by the change of signal and noise caused by the change of structure and external conditions, which limit the accuracy of damage location [15]. In addition, due to the dispersion characteristics of Lamb wave, the damage scattering wave will be distorted in the process of propagation, which will also affect the determination of the propagation time of the damage scattering signal. Therefore, the dependence on the baseline signal reduces the effectiveness and accuracy of damage identification.

In order to reduce the dependence on the baseline signal, a time reversal technique was developed for damage detection [16-18]. The time reversal method is based on the principle of acoustic reciprocity to achieve adaptive focusing and detection of acoustic waves without prior knowledge of the properties and structures of media and transducer arrays. The sensor reverses the received time-domain signal from the actuator, and then transmits the reversal signal. That is to say, signal is first received and later sent, later received and first sent. This method has been proved to be effective in compensating the dispersion effect of Lamb waves [19,20]. Based on time reversal theory, the acoustic source signal can be focused in time and space by the focused acoustic emission signal without considering the influence of waveform modes. The signal-to-noise ratio of the detection signal is effectively improved as the noise signal cannot be focused. The time reversibility of Lamb wave has been applied to damage identification [21,22]. But it requires precise wave velocity and propagation time to build damage image. Especially when there are many damages, it is difficult to extract wave packet information as wave packet aliasing happens due to model conversion of Lamb wave. And the uncertainty of damage location caused by measurement error and model error in practical application is inevitable.

The damage probability imaging method has been widely studied by researchers, which uses the sparse sensor networks for damage imaging without the need of velocity and propagation time of guided wave. Zhao [23] proposed a damage probability imaging method based on correlation analysis, which constructs damage distribution probability map by using signal difference coefficient. Wang [24] improved the performance of the algorithm, which combined the damage probability imaging method based on correlation analysis and the virtual sensing path. The algorithm is verified by identifying multiple incisions. Wu [25] studied the effects of several parameters on damage identification in damage probability imaging method, and proposed some methods to determine these parameters. Hua [26] proposed a damage probability imaging method based on local signal difference coefficient to improve the quality of damage imaging. In the above studies of damage probability imaging methods, damage imaging is based on a relatively inaccurate probability of damage distribution. For the damage distribution probability of a sensor-actuator channel, wherever the real damage is located, it is closer to the direct path of the sensor-actuator channel, which means that the probability of damage always reaches the maximum on the direct path of sensor-actuator channel. The damage distribution probability in above methods is an inaccurate distribution probability, which need the structural health signal as the baseline signal, and use the difference of the baseline signal and the detection signal as the damage factor for determination of the damage location in the structure and other information. Therefore, these problems will lead to the reduction of the accuracy of damage location and limit the application of damage probability imaging method in practical engineering structures.

In order to improve the accuracy of damage location and reduce the dependence on the baseline signal, a baseline-free time reversal probabilistic imaging algorithm (BFTRPI) is proposed, which uses the relative distance between the damage distance excitation and the direct path of the sensor channel. The damage probability method is used for damage imaging of multiple damages in the aluminium plate, and the experimental verification research is carried out.

The rest of paper is organized as follows. Section 2 introduces the time reversal theory. The damage imaging algorithm is derived in Section 3. Experimental research and result analysis are presented in Section 4. Finally the conclusion is drawn in Section 5.

2. Time reversal theory

The time reversal focusing process of Lamb wave is shown in Fig. 1, where A acts an actuator and B as a sensor. Firstly, the excitation voltage signal $I(w)$ is loaded on the actuator A, and the response signal $V_{P2}(w)$ to sensor B is propagated through the structure. The response signal can be expressed as follows:

$$V_{P2}(r,w) = I(w)K_{P1}(w)K_{P2}(w)G(r,w) \tag{1}$$

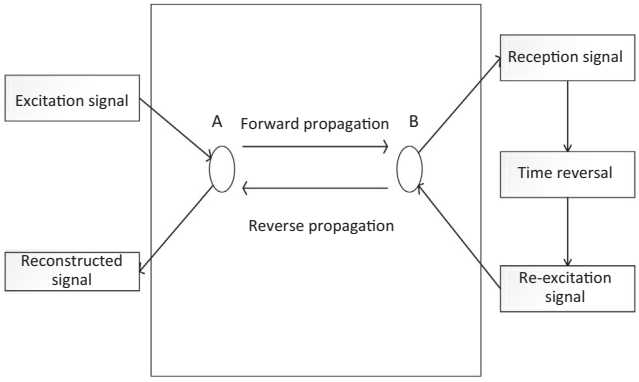

Fig. 1. The schematic diagram of the time reversal process of Lamb wave signals.

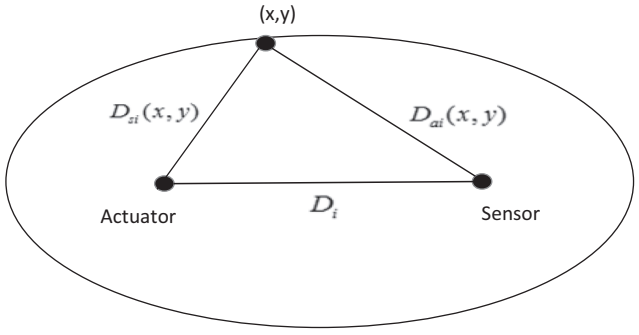

Fig. 2. Illustration of relative distance R_i.

机电耦合系数

where $K_{P1}(w)$and$K_{P2}(w)$ are the Electromechanical Coupling Coefficient of PZT1 and PZT2, respectively. $G(r,w)$ is the frequency response transfer function of the structure. The response signal is inverted in time domain. As inversion in time domain corresponds to conjugate in frequency domain, the response signal is expressed as:

频率响应传递函数

共轭

$$\hat{V}^*_{P2}(r,w) = I^*(w)K^*_{P1}(w)K^*_{P2}(w)G^*(r,w) \tag{2}$$

According to the reciprocity of acoustic wave propagation, the positions of sensors and actuators are reciprocal, and the reciprocal structures have the same frequency response transfer function. The structural response signal received by PZT1 is expressed as:

互换、互易性

$$\begin{aligned} V_{P1}(r,w) = &\ K_{P1}(w)\hat{V}^*_{P2}(r,w)K_{P2}(w)G(r,w) \\ = &\ I^*(w)K^*_{P1}(w)K^*_{P2}(w)G^*(r,w)K_{P1}(w)K_{P2}(w)G(r,w) \\ = &\ I^*(w)K^*_{P12}(w)K_{P12}(w)G^*(r,w)G(r,w) \end{aligned} \tag{3}$$

where$K_{P12}(w)$is the product of$K_{P1}(w)$and$K_{P2}(w)$. It is noticed that $K^*_{P12}(w)K_{P12}(w)G^*(r,w)G(r,w)$ is a conjugate complex multiplication. Its inverse Fourier transform at the time zero is superimposed, and the peak value of the main correlation can be obtained.

The Lamb wave characteristics in plate structures are further analyzed. According to the Lamb wave model, the frequency response transfer function can be expressed in the following frequency domain form:

频率响应传递函数

$$\begin{aligned} &G(r,w) = \textstyle\sum_{A_i} a_{A_i}(r,w)e^{-jk_{A_i}r} + \sum_{S_i} a_{S_i}(r,w)e^{-jk_{S_i}r} \\ &k_{A_i} = \tfrac{w}{c_{A_i}}, k_{S_i} = \tfrac{w}{c_{S_i}} \end{aligned} \tag{4}$$

where A_i and S_i represent the i-th anti-symmetric mode and symmetric mode, respectively. $a_{A_i}(r,w)$, k_{A_i} and c_{A_i} represent the signal amplitude, wave number and propagation speed of$A_i$mode, respectively. And$a_{S_i}(r,w)$, $k_{S_i}$and c_{S_i}represent the signal amplitude, wave number and propagation speed of $S_i$mode, respectively. When only modes $A_0$and S_0mode exist, the structural response signal $V_{P1}(w)$ can be expressed as:

$$\begin{aligned} &V_{P1}(w) = I^*(w)|K_{P12}(w)|^2(a_{A_0}(r,w)e^{-jk_{A_0}r} + \\ &a_{S_0}(r,w)e^{-jk_{S_0}r})(a_{A_0}(r,w)e^{jk_{A_0}r} + a_{S_0}(r,w)e^{jk_{S_0}r}) \\ &= I^*(w)|K_{P12}(w)|^2[a^2_{A_0}(r,w) + a^2_{S_0}(r,w) + \\ &a_{A_0}(r,w)a_{S_0}(r,w)](e^{-j(k_{S_0}-k_{A_0})r} + e^{j(k_{S_0}-k_{A_0})r}) \end{aligned} \tag{5}$$

The inverse Fourier transform for the above signals can be expressed as:

$$\begin{aligned} V_{P1}(t) = &\frac{1}{2\pi}\int_{-\infty}^{\infty} I^*(w)|K_{P12}(w)|^2 G(r,w)G^*(r,w)e^{jwt}dw \\ = &\frac{1}{2\pi}I(-t)|K_{P12}|^2\left[a^2_{A_0}+a^2_{S_0}\right] \\ &+\frac{1}{2\pi}|K_{P12}|^2 a_{A_0}a_{S_0}\left\{\hat{I}\left[r\left(\frac{1}{c_{A_0}}-\frac{1}{c_{S_0}}\right)-t\right]+\hat{I}\left[r\left(\frac{1}{c_{S_0}}-\frac{1}{c_{A_0}}\right)-t\right]\right\} \end{aligned} \tag{6}$$

From Eq. (6), it is seen that the signal obtained at the source after time reversal can be divided into two parts, when there are only mode A_0 and mode S_0 Lamb wave. One is the time reversal signal with zero-time amplitude of $\frac{1}{2\pi}|K_{P12}|^2[a^2_{A_0}+a^2_{S_0}]$, and the amplitude is the correlation superposition of two mode signals, which is the focus of each mode signal and the main peak of the whole signal.?? If the inverse Fourier transform $V_{P1}(t)$ is inverted in time domain, part of the signal has the same form as the intense signal, but difference amplitude. Therefore, the zero-time main peak can also be regarded as the reconstruction of the original intense signal. The other part is the back signal at $\pm\left(\frac{r}{c_{A_0}}-\frac{r}{c_{S_0}}\right)$ time with the amplitude of $\frac{1}{2\pi}|K_{P12}|^2 a_{A_0}a_{S_0}$. It can be seen that the signal amplitude of this part is less than the zero time amplitude. There is no overlap, only the side lobe of the signal. It can be seen that signal focusing by a single sensor/actuator pair can only be achieved through time reversal in the field of ultrasound.

When there are multiple sensor elements in the structure and only mode $A_0$and mode S_0Lamb are excited in the structure, the signal obtained on the$i$-th sensor element $R_i$can be expressed as:

$$\begin{aligned} V_{R_i}(r_i) = &\ I(w)K_AK_{R_i}G_i(r_i) \\ = &\ I(w)K_{AR_i}\left(a_{A_0}(r_i)e^{-jk_{A_0}r_i} + a_{S_0}(r_i)e^{-jk_{S_0}r_i}\right) \end{aligned} \tag{7}$$

where K_A and K_{R_i} are the Electromechanical Coupling Coefficients of the i-th actuator and sensor respectively, which are related to the frequency of the intense signal, $K_{AR_i}$is the product of K_A and K_{R_i}, and r_i is the distance from the$i$-th sensor to the actuator.

When the monitoring signal is time reversed and loaded on the corresponding sensor, the signal obtained from the structural response signal $V_{P1}(w)$ and the excitation element P_a is shown as:

$$\begin{aligned} &V_A(w) = \textstyle\sum_i I^*(w)\left|K_{Ar_i}(w)\right|^2[a^2_{A_0}(r_i) + a^2_{S_0}(r_i) + \\ &a_{A_0}(r_i)a_{S_0}(r_i)\left(e^{-j(k_{S_0}-k_{A_0})r_i} + e^{j(k_{S_0}-k_{A_0})r_i}\right)] \end{aligned} \tag{8}$$

Inverse Fourier transformation can be obtained:

$$\begin{aligned} V_A(t) = &\frac{1}{2\pi}\sum_i |K_{AR_i}|^2[a^2_{A_0}(r_i)+a^2_{S_0}(r_i)]I(-t)+\frac{1}{2\pi} \\ &\times\sum|K_{AR_i}|^2 a_{A_0}(r_i)a_{S_0}(r_i)\left\{\hat{I}\left[r_i\left(\frac{1}{c_{A_0}}-\frac{1}{c_{S_0}}\right)-t\right]+\hat{I}\left[r_i\left(\frac{1}{c_{S_0}}-\frac{1}{c_{A_0}}\right)-t\right]\right\} \end{aligned} \tag{9}$$

The signal in the above equation can be divided into two parts. The first part is the zero-time main peak, which not only focuses multiple modes of each monitoring signal, but also focuses each monitoring signal. The peak amplitude increases significantly. In the second part, the side lobe peaks do not overlap and sometimes cancel each other because of the different distance$r_i$between the sensing elements and the exciting elements.

Damage can be regarded as a secondary wave source in the process of Lamb wave signal propagation. The damage information can be obtained by analyzing the damage scattering signal, by using the principle of active Lamb wave structural health monitoring method. However, the energy and amplitude of the damage scattering signal are usually small, which is easy to be submerged by noise and lead to the low signal-to-noise ratio of the signal. The

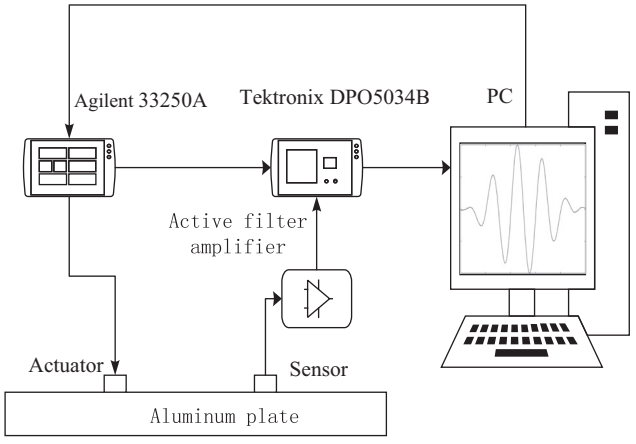

Fig. 3. Experimental block diagram.

signal focusing at the source can be achieved by responding to the back-loading of the signal. Therefore, the back-loading of the damage scattering signal should focus on the damage to enhance the signal, which is the basis of the back-enhancement of the signal-to-noise ratio of the damage scattering signal. Besides the damage scattering signal, there are other signals, such as noise, boundary reflection or scattering signal. These responses have different sources and occurring time, and nonuniform focus when time reversal loading applies, so it is only random superposition which can not achieve enhancement. From Eq. (9), the energy of damage scattering signal in monitoring signal can be enhanced, and the signal-to-noise ratio can be improved.

It should be noted that the damage is considered as a point in the derivation process, the damage scattering signals received by the sensors are considered as signals from the same point. However, the practical damage has a certain size, which also causes the difference between relative positions of the sensors and the damage, thus leads to a small deviation in the scattering points of the scattering signals of the sensors. The direct propagation signal and boundary reflection signal can be eliminated by applying an appropriate time window function to the monitoring signal, and only the internal scattering signal can be retained. At this time, in the internal scattering signals of each pair of piezoelectric sensors, all the damage scattering signals come from the same damage with the same wave source location. When the signal is loaded after time reversal, it can focus at the same position.

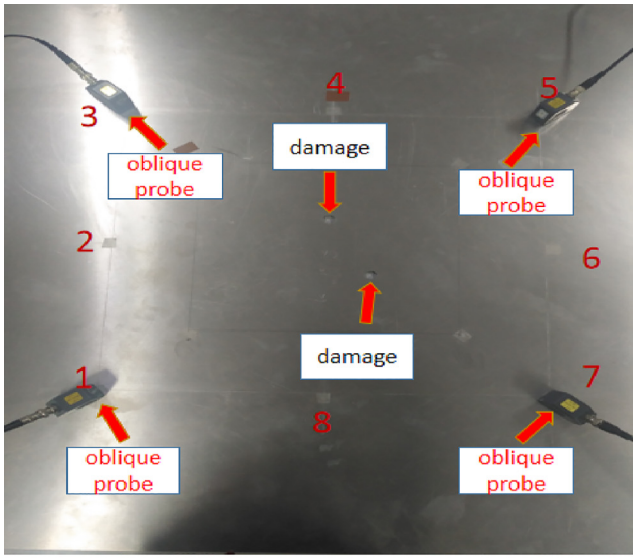

(a)

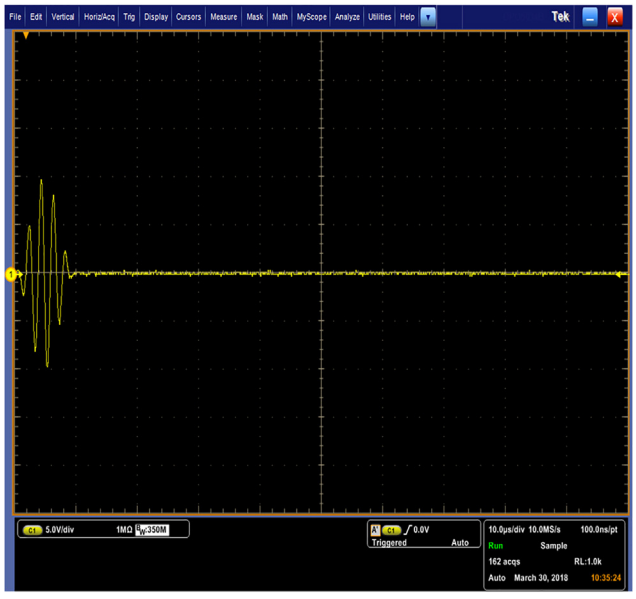

(b)

Fig. 4. (a)Experimental diagram of oblique probe and defect position. (b)Exciting signal.

3. Damage imaging algorithm

When using the time reversal method to detect signal reconstruction, the damage on the sensing path will introduce nonlinear factors, which will make time reversal reconstruction ineffective in some extent. By comparing the reconstructed signal with the original excitation signal, the damage on the path can be evaluated. Soho [27] studied the relationship between the shape consistency of the two signals and the damage situation, and proposed a damage factor to characterize the damage situation, which is expressed as:

$$f_i = 1 - \frac{\left|\int_{t_0}^{t_1} I_i(t)V_i(t)dt\right|}{\sqrt{\int_{t_0}^{t_1} I_i^2(t)dt \int_{t_0}^{t_1} V_i^2(t)dt}} \tag{10}$$

where $I_i(t)$ and $V_i(t)$ represent the original intense signal and time-reversal reconstructed signal on the i-th sensor path, respectively. The damage factor ranges from 0 to 1. And a non-zero real constant k is defined. When $V_i(t) = kI_i(t)$, $f_i = 0$, the shape of the two signals is identical, which means that there is no damage on the sensor path. The larger the f_i value, the greater the distortion of the two signal waveform, which means the probability of damage on the sensing path increases. The damage factor is only affected by the non-linear factors introduced by the damage, and no baseline signal is required. By enlarging the time reversal window, the detection range can be widened.

In damage probability imaging method, the monitoring area is divided into uniformly distributed pixels. The probability of damage for each pixel is obtained by superposing the elliptical influence regions of the damage factors of each excitation-sensing channel. The maximum pixel value is the damage location.

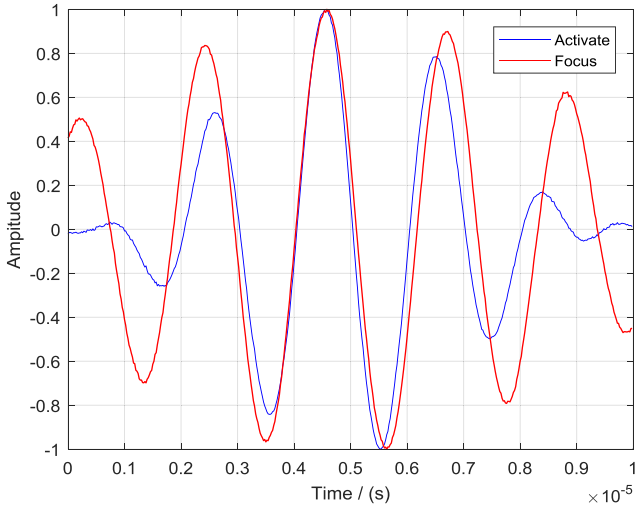

Fig.5. Comparison of excitation signal and focus signal.

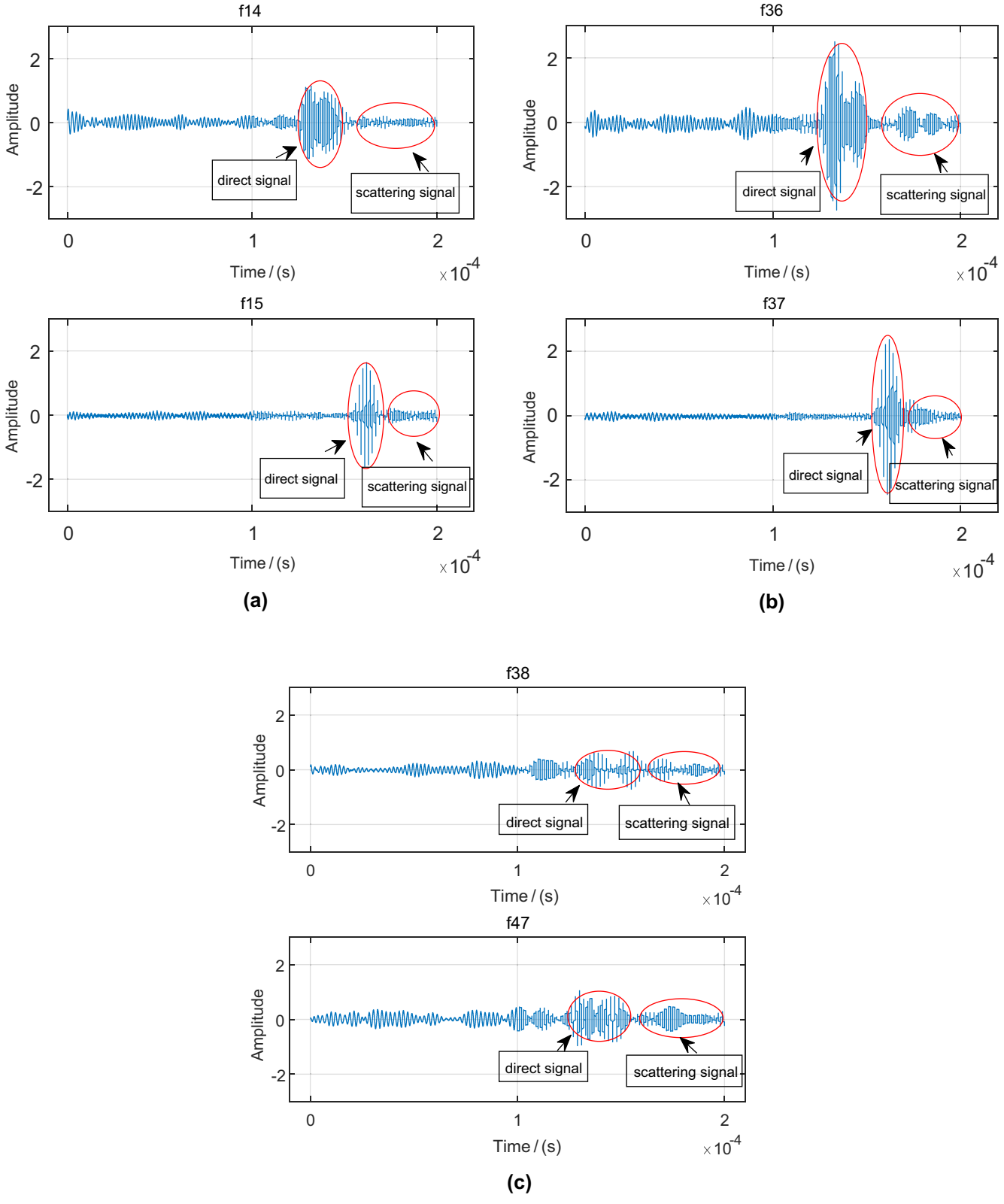

Fig. 6. Structural response signal. (a), (b) and (c) are the response signal of each sensor-actuator path.

In this paper, the damage location accuracy is modified by the weight distribution function. The farther the damage from the direct path of the sensor-actuator channel, the smaller the impact of the damage on the guided wave signal of the sensor-actuator channel. Therefore the relative distance between the damage and the direct path of other sensor-actuator channels can be deter-

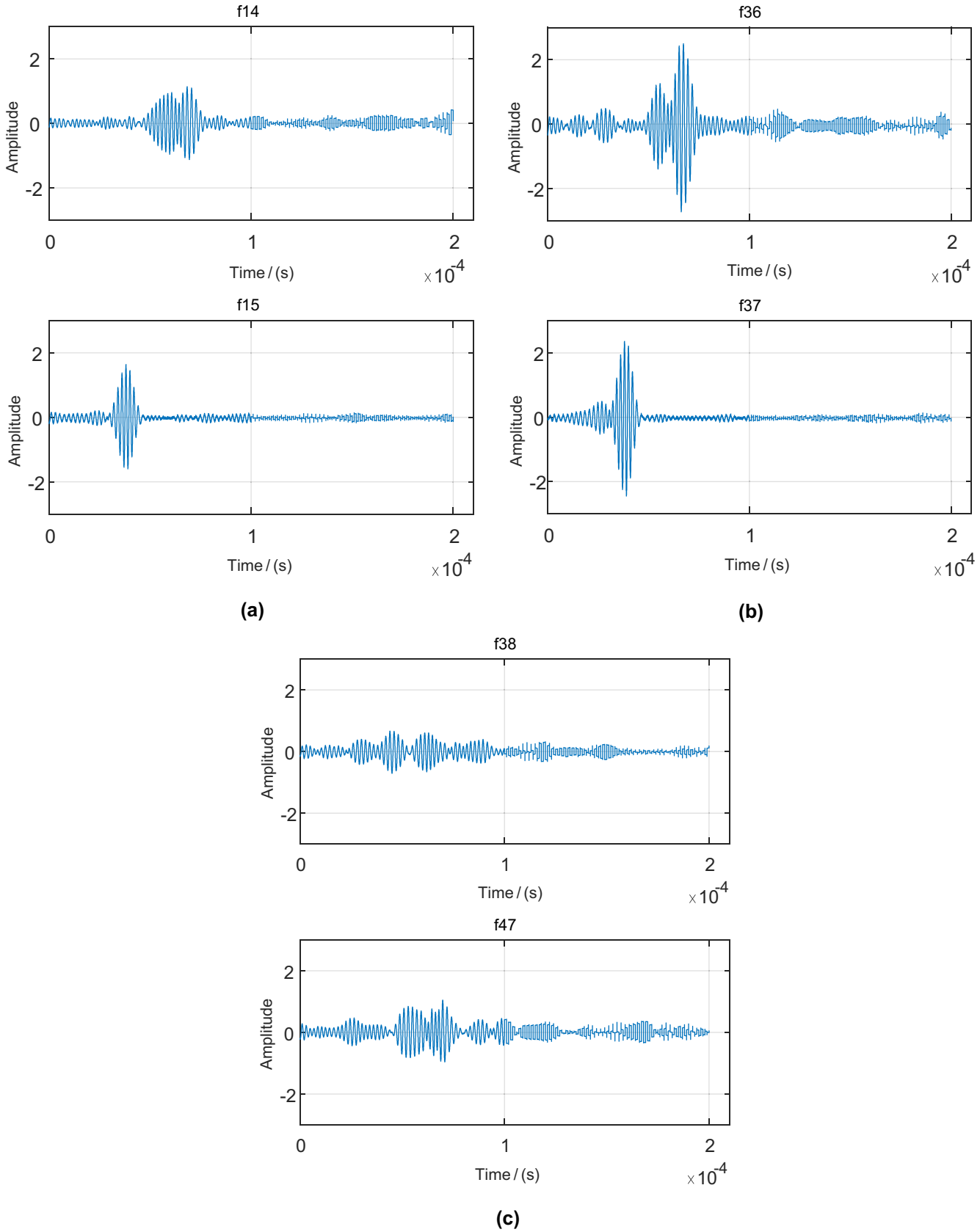

Fig. 7. Time reversal signal. (a), (b) and (c) are the time reversal signal of each sensor-actuator path.

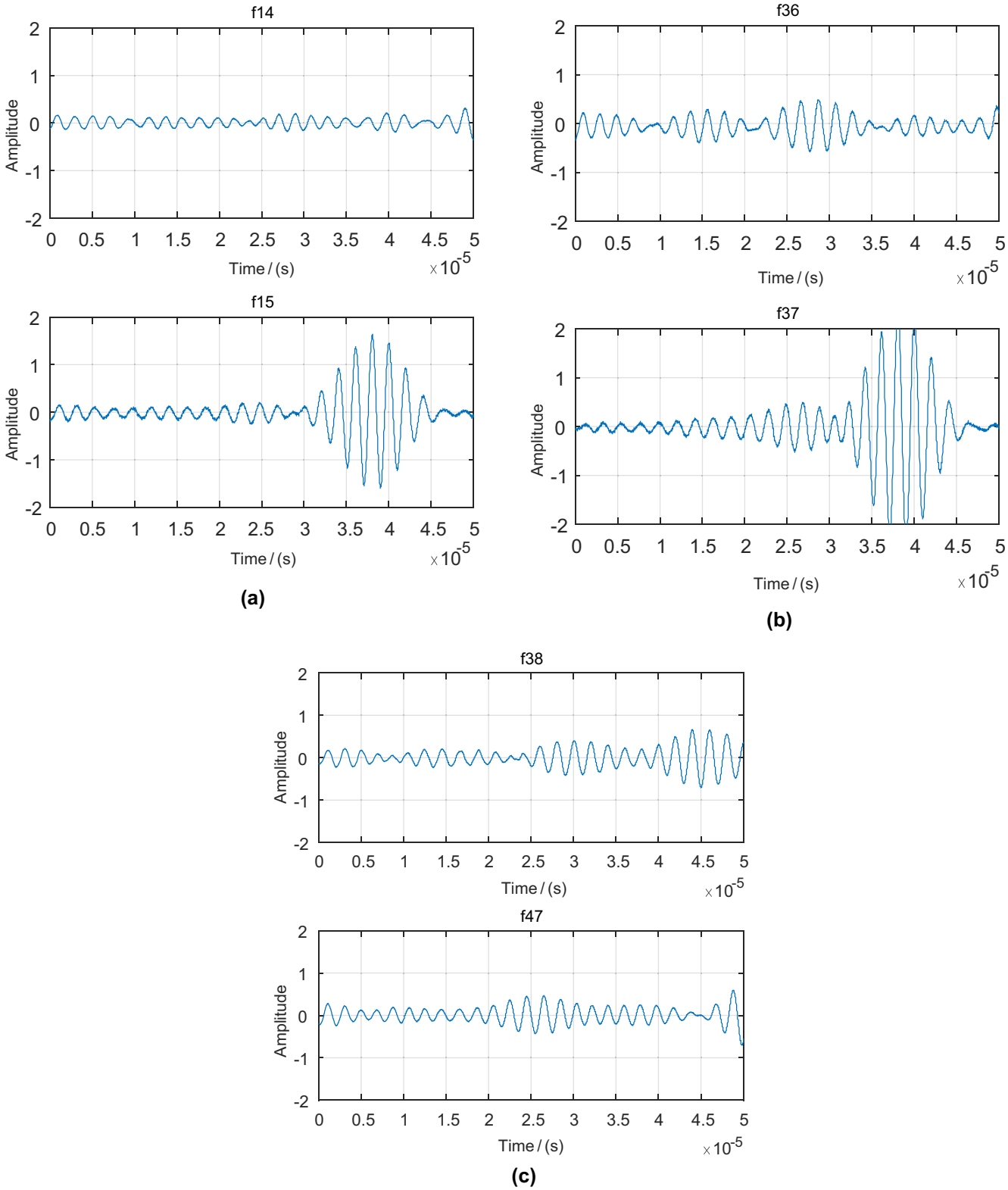

Fig. 8. Time reversal scattering excitation signal. (a), (b) and (c) are the time reversal scattering signal of each sensor-actuator path.

mined by the relative size of damage factor. On these relative distances, the probability of damage is the greatest. When leaving these locations, the probability of damage decreases gradually.

Assuming that there are N sensor-actuator channels in the monitoring area, the probability of damage to the pixels is expressed as:

$$P(x,y) = \sum_{i=1}^{N} f_i \cdot W_{Mi}[R_i(x,y)] \tag{11}$$

$W_{Mi}[R_i(x,y)]$ is the weight distribution function of the$i$-th sensor-actuator channel, which can be expressed as:

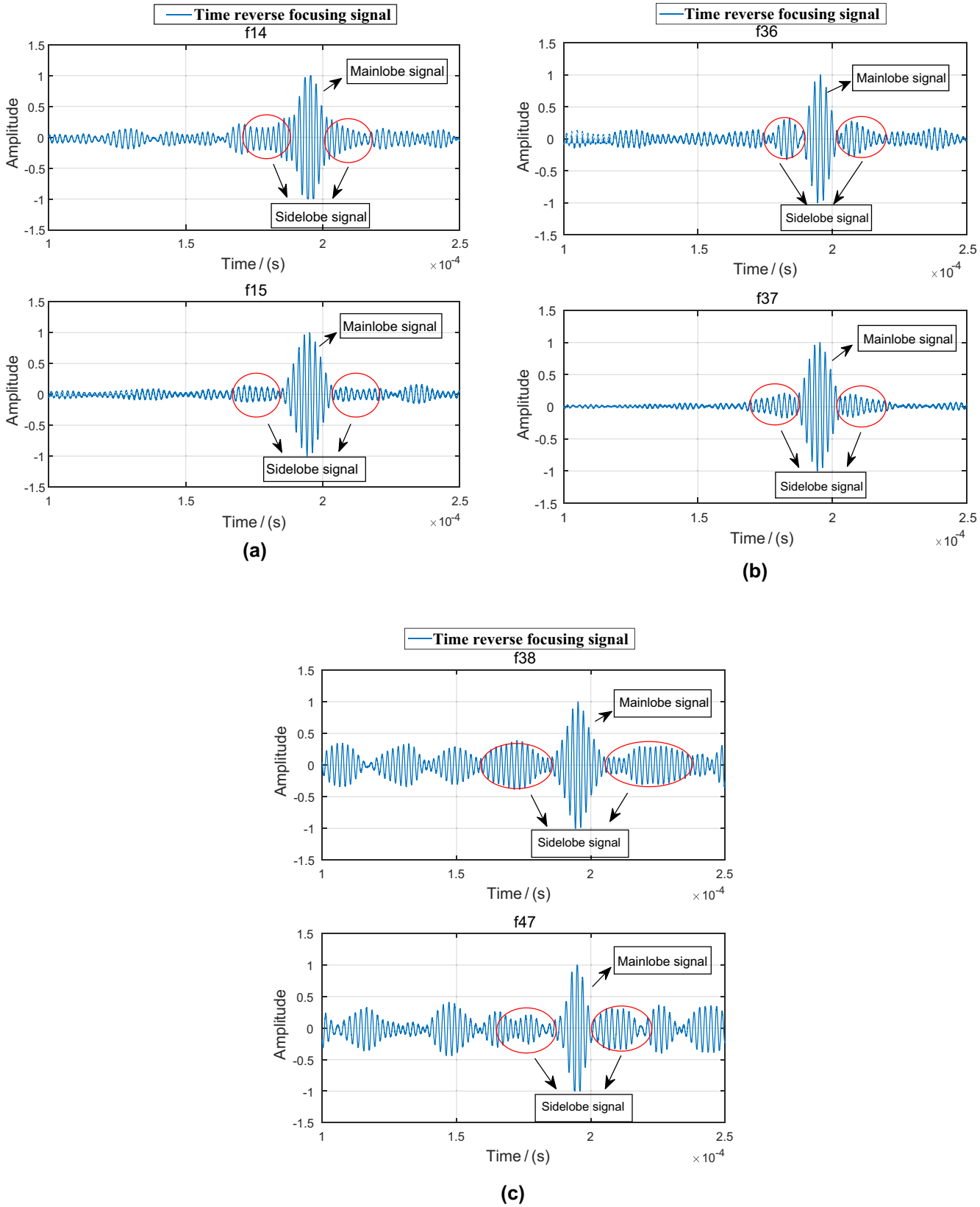

Fig. 9. Excitation signal after time reversal. (a), (b) and (c) are the response signal of each sensor-actuator path after time reversal.

$$W_{Mi}[R_i(x,y)] = \begin{cases} 1 - \left[\frac{R_i(x,y)}{\beta} - \left(1 - \frac{f_i}{f_{\max}}\right)\right], \left(1 - \frac{f_i}{f_{\max}}\right)\beta \leqslant R_i(x,y) < \left(2 - \frac{f_i}{f_{\max}}\right)\beta \\ 1 + \left[\frac{R_i(x,y)}{\beta} - \left(1 - \frac{f_i}{f_{\max}}\right)\right], R_i(x,y) < \left(1 - \frac{f_i}{f_{\max}}\right)\beta \\ 0, R_i(x,y) \geqslant \left(2 - \frac{f_i}{f_{\max}}\right)\beta \end{cases} \tag{12}$$

where $f_{\max}$ is the maximum damage factor in all sensor-actuator channels. The maximum value of the weight distribution function $W_{Mi}[R_i(x,y)]$ is located at the $R_i(x,y)$, and Its pixel is $\left(1 - \frac{f_i}{f_{\max}}\right)\beta$. The value of weight distribution function $W_{Mi}[R_i(x,y)]$ decreases gradually as the pixel (x,y) is far away from the pixel $R_i(x,y) = \left(1 - \frac{f_i}{f_{\max}}\right)\beta$, and the weight distribution function $W_{Mi}[R_i(x,y)]$ depends on $R_i(x,y)$. This function is the relative distance between the pixel (x,y) and the i-th sensor-actuator channel. As shown in Fig. 2., when the result of formula 13 is 1, the pixel is directly in the sensor path. When the result of formula 13 is β, the pixel is located at the edge of the ellipse.

为0时？

$$R_i(x,y) = \frac{D_{ai}(x,y) + D_{si}(x,y)}{D_i} - 1 \tag{13}$$

where D_i is the distance between the actuator and the sensor of the i-th sensor-actuator channel; $D_{ai}(x,y)$ and $D_{si}(x,y)$ are the distance between the actuator and the sensor of the first sensor-actuator channel from the pixel (x,y), respectively.

4. Experimental research and result analysis

The experimental device is shown in Fig. 3. An excitation signal is generated by a 33250A function generator manufactured by Agilent company. The initial excitation signal is applied to the excitation sensor through an arbitrary signal generator, and the panel settings of the signal generator are adjusted to ensure that the excitation waveform is in the form of narrow-band pulse, and the waveform of the excitation signal is observed by an oscilloscope. Then, the mechanical wave propagated is converted into electrical signal by the receiving sensor. After amplification by an active filter amplifier, the received signal is observed by the oscilloscope. The time window T is roughly determined by the propagation distance of waveform, and the signal is transmitted to the PC. At last, the collected Lamb wave signals are time reversed in the corresponding time window. The data after time reversal are imported into the software of waveform generator to draw the waveform of time reversal Lamb wave.

A 1000 mm × 1000 mm × 1.5 mm aluminum plate is used for experiment. A sensor-actuator network with eight piezoelectric sensors is constructed by the piezoelectric effects of piezoelectric sensor. Their coordinates were 1#(250 mm, 250 mm), 2#(250 mm, 500 mm), 3#(250 mm, 750 mm), 4#(500 mm, 750 mm), 5#(750 mm, 750 mm), 6#(750 mm, 500 mm), 7#(750 mm, 250 mm), and 8#(500 mm, 250 mm), respectively. There are only four channels in the oscilloscope. One oblique probe acts as actuator and the other three acts as sensors. The oblique probe collects data at each response position in turn, as shown in Fig. 4(a). The excitation signal is a 5 cycles Hanning window tone burst with frequency of 200 kHz, as shown in Fig. 4(b). When the exciter is loaded perpendicular to the surface of the plate, Lamb wave generated is mainly in S0 mode, and the sampling frequency of the response signal was set to 20 MHz. The form of two damages is through hole with a diameter of 15 mm. Central positions of the two damages are (450 mm, 500 mm), and (550 mm, 550 mm), respectively. Firstly, the structural response signals under the initial narrow-band excitation are collected, and then the response signal is intercepted by window function according to the relative position of the sensor-actuator combination and the boundary of each monitoring channel. Only the direct and internal scattering signals are retained, and the intercepted signals are time reversed and loaded twice. Finally, the structural response signals with time reversal focus are obtained.

Fig. 5 shows the comparison between the normalized focusing signal and the excitation signal of the$S_4 - S_7$ sensing path for double defects. It can be seen that the reconstructed waveform has obvious dispersion. In this paper, the data of six paths with the highest damage factor are used for damage location imaging.

The wave source is focused by time reversal method to verify the method's validity. To locate the damage accurately, the waveform information generated by the passive source of damage should be intercepted as completely as possible to avoid the influence of excitation signal on the location. Fig. 6 shows the structural response signal. The $f_{14}, f_{15}, f_{36}, f_{37}, f_{38}$ and f_{47} are the received signal of each sensor, with maximum damage factor in their sensing paths. The first letter of the subscript is the actuator number, and the second letter represents the receiving sensor number. It can be seen that there are direct propagation signal and scattering signal in the response signal. The scattering signal contains the possible mode conversion signal. The scattering signals caused by two damages overlap with each other, and also overlap with the direct signals. Due to the interference of noise, it is difficult to distinguish and identify the scattering signals. Compared with the excitation signal, the structural response signal shows the wave packet continuation problem caused by the dispersion effect. The position and energy of heavy wave packet of each signal is different. It should be emphasized that because the dispersion effect is sensitive to the frequency bandwidth, narrowing the pulse width of the excitation signal (such as reducing the cycle number of the narrow-band excitation signal) will reduce the frequency resolution of the excitation signal, which leads to enhancement dispersion effect and more significant wave packet continuation. The problem of wave packet aliasing can not be fundamentally solved. Fig. 7 is the time reversal signal.

The scattering signals are truncated by a window function based on the distance between sensors, actuators and boundary in each monitoring path. The waveform is shown in Fig. 8. The six signals in Fig. 6 are truncated to get the damage scattering signal, and the time reversal signal is used as the excitation signal.

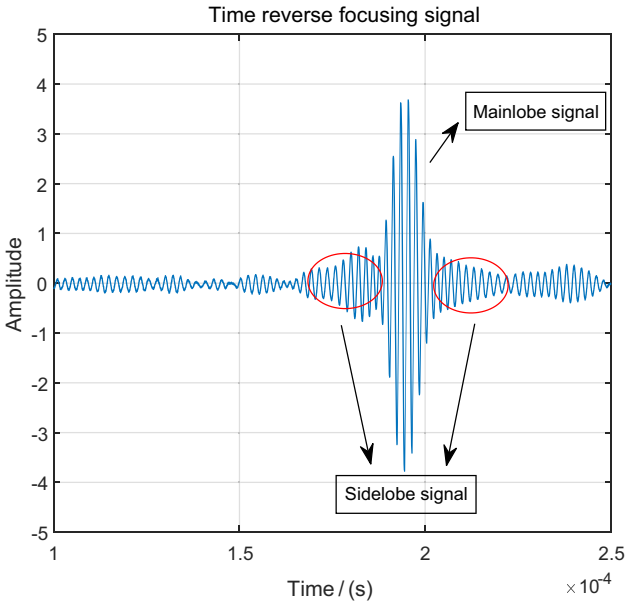

Fig. 10. Time reversal focusing signal.

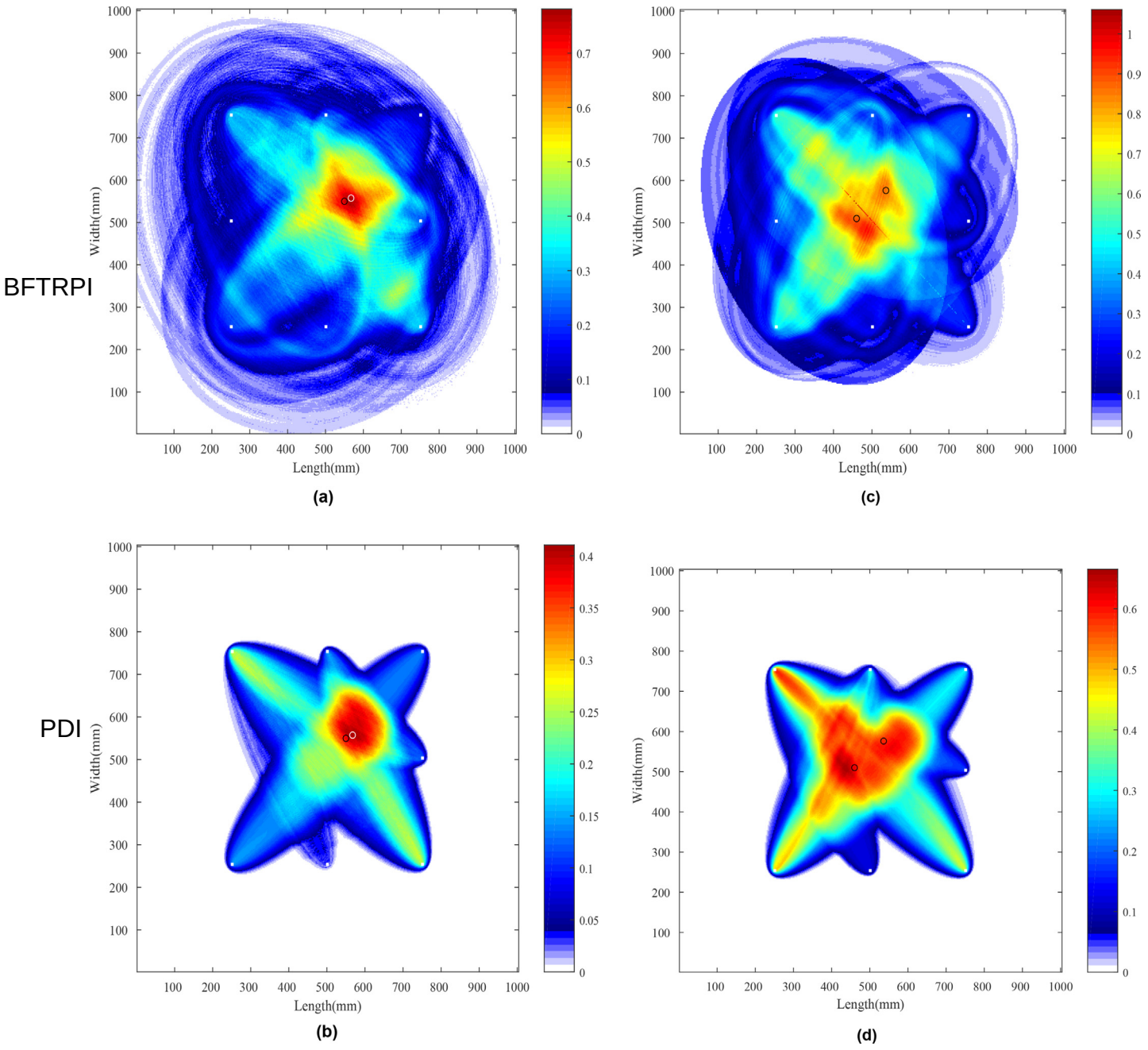

Fig. 11. Damage location results. (a) and (c) Damage imaging using the BFTRPI algorithm for single damage and two damages. (b) and (d) Damage imaging using the traditional PDI algorithm for single damage and two damages.

The six sets of structural response signals are processed by time reversal loading, and the time reversal focusing signals are obtained, as shown in Fig. 9. It is seen that the dispersion effect in the original response signal is reduced, the wave packet pulse is re-compressed in time domain, and each wave packet is separated. The structural response signal in Fig. 8 is reloaded by time reversal, and the focusing result is shown in Fig. 10. The main lobe and side lobe of signal $f_{36}$are still clearly visible after time reversal due to its independence and distinctness. The main lobes of other scattering signals are obvious, but the side lobes are not obvious. This is due to the overlapping of direct signals and scattering signals caused by the model transformation and difficulty of extracting scattering signals for multiple damages. It should be pointed out that time reversal focusing is not applicable for signal changes caused by noise, system errors and human errors. Therefore, in the process of time reversal focusing, the signal changes are only random superimposition, can not be amplified and compensated, and even cancel each other, which reduces the impact on useful signals.

时间反转只会叠加损伤波源信号，对噪声和人认为误差不叠加

The validity of the time reversal theory is verified by experiments. The damage signal can be inverted by time reversal and the wave source can be focused.

The imaging by The BFTRPI algorithm and traditional probability-based diagnostic imaging algorithm (PDI) is shown in Fig. 11. The white circle is the real damage location, and the black circle is the estimated damage location by the algorithm. From the Fig. 11 (a) and (b), both of these algorithms have high positioning accuracy for the single damage. Therefore, single damage location can not reflect the location effect of two algorithms. We need to

locate multiple damages to verify the effectiveness of the algorithm.

The highlighted part of the imaging is the area with the greatest damage probability. It can be seen that the damage location and area monitored by the imaging basically reflect the actual damage situation. The positioning accuracy of BFTRPI algorithm is obviously higher than that of traditional PDI algorithm. The estimated position by BFTRPI algorithm is closer to the actual damage position. The location area of damage and artifact area for traditional PDI algorithm are both higher than that of BFTRPI algorithm.

5. Conclusion

In this paper, the time reversal method of Lamb wave and damage probability are used to study the baseline-free damage monitoring of active Lamb wave, and a baseline-free time reversal probabilistic imaging algorithm is proposed. Aiming at the shortcomings of existing damage detection methods based on baseline signals, this method utilizes the focusing principle of time reversal on wave sources to reconstruct the structural response signals in time reversal for eliminating the influence of the dispersion effect of Lamb waves. Based on the relationship between damage factor and relative distance between damage distance excitation and direct path of sensor channel, multiple damages identification and location on aluminum plate are carried out, which is combined with damage probability distribution function in damage probability imaging method. The effectiveness of the proposed method is verified. The experimental results show that the structural response signal is directly processed under the current state, the dependence on the baseline signal is eliminated, and the monitoring results have better accuracy. The accuracy of damage location is higher than that of the traditional damage probability imaging algorithm. The proposed method effectively identifies the multiple damages and improves the practicability of Lamb wave health monitoring technology, which shows great significance in practical application. In the future, we will continue to analyze and study this method, and use the time reversal method and Probabilistic Damage imaging method to judge the shape and size of the damage.

Acknowledgment

This work was supported by the National Natural Science Foundation of China (Grant No. 61671285, 11674214,11874255).

References

[1] Carrino Stefano, Nicassio Francesco, Scarselli Gennaro, et al., Finite difference model of wave motion for structural health monitoring of single lap joints [J], Int. J. Solids Struct. 161 (2019) 219–227.
[2] B. Zoubi Ahmad, Kim Sungwon, O. Adams Daniel, et al., Lamb wave mode decomposition based on cross-Wigner-Ville distribution and its application to anomaly imaging for structural health monitoring [J]., IEEE Trans. Ultrason. Ferroelectr. Freq. Control 3 (2019) 193–208.
[3] J.Y. Park, J.R. Lee, Application of the ultrasonic propagation imaging system to an immersed metallic structure with a crack under a randomly oscillating water surface[J], J. Mech. Sci. Technol. 31 (9) (2017) 4099–4108.
[4] Y. Sidibe, F. Druaux, D. Lefebvre, et al., Signal processing and Gaussian neural networks for the edge and damage detection in immersed metal plate-like structures[J], Artif. Intell. Rev. 46 (3) (2016) 289–305.
[5] Yu.Lu. Hanfei Zhang, Shiwei Ma, et al., Adaptive sparse reconstruction of damage localization via Lamb waves for structure health monitoring [J], Computing 101 (6) (2019) 679–692.
[6] Migot Asaad, Bhuiyan Yeasin, Giurgiutiu Victor, Numerical and experimental investigation of damage severity estimation using Lamb wave-based imaging methods [J], J. Intell. Mater. Syst. Struct. 30 (4) (2019) 618–635.
[7] Radzienski Maciej, Kudela Paweł, Marzani Alessandro, et al., Damage identification in various types of composite plates using guided waves excited by a piezoelectric transducer and measured by a laser vibrometer [J], Sensors 19 (9) (2019) 1958.
[8] Moriot Jeremy, Quaegebeur Nicolas, Le Duff Alain, et al., A model-based approach for statistical assessment of detection and localization performance of guided wave-based imaging techniques [J]., Struct. Health Monit.-AN Int. J. 17 (6) (2019) 1460–1472.
[9] Shungen Xiao, Shulin Liu, Feng Jiang, Mengmeng Song, Shouguo Cheng, Nonlinear dynamic response of reciprocating compressor system with rub-impact fault caused by subsidence [J], J. Vib. Control 25 (11) (2019) 1737–1751.
[10] Esfandabadi Yasamin Keshmiri, De Marchi Luca, Testoni Nicola, et al., Full wavefield analysis and damage imaging through compressive sensing in lamb wave inspections [J], . IEEE Trans. Ultrason. Ferroelectr. Freq. Control 65 (2) (2018) 269–280.
[11] Zhang Haiyan, Ma. Shiwei, Feng Guorui, et al., Probability damage imaging in Lamb wave structural health monitoring [J], Acta Acustica 37 (4) (2012) 401–407.
[12] Jiao Jingpin, Du Li, Li Yongqiang, et al., Study on the compound imaging method for crack detection in plate structure using array of Lamb waves [J], Chinese J. Sci. Instrum. 37 (3) (2016) 593–601.
[13] Hoon Sohn, Effects of environmental and operational variability on structural health monitoring[J], Philos. Trans. R. Soc. A: Math. Phys. Eng. Sci. 2007 (365) (1851) 539–560.
[14] Kapuria Santosh, Agrahari Jitendra Kumar. Shear-lag solution for excitation, sensing, and time reversal of Lamb waves for structural health monitoring[J], J. Intell. Mater. Syst. Struct. 29 (4) (2018) 585–599.
[15] Agrahari Jitendra Kumar, Kapuria Santosh. Active detection of block mass and notch-type damages in metallic plates using a refined time-reversed Lamb wave technique[J], Struct. Control Health Monit. 25 (2) (2018) e2064.
[16] R.K. Ing, M. Fink, Time-reversed Lamb waves [J], IEEE Trans. Ultrason. Ferroelectr. Freq. Control 45 (4) (1998) 1032–1043.
[17] Y. Jun, U. Lee, Computer-aided hybrid time reversal process for structural health monitoring[J], J. Mech. Sci. Technol. 26 (1) (2012) 53–61.
[18] C. Chen, Y. Li, F.G. Yuan, Impact source identification in finite isotropic plates using a time-reversal method: experimental study[J], Smart Mater. Struct. 21 (10) (2012) 105025.
[19] H.W. Park, S.B. Kim, H. Sohn, Understanding a time reversal process in Lamb wave propagation[J], Wave Motion 46 (7) (2009) 451–467.
[20] H. Sohn, C.R. Farrar, Damage detection in composite plates by using an enhanced time reversal method[J], J. Aerosp. Eng. 20 (3) (2007) 141–151.
[21] Zhao Xiaoliang, Gao Huidong, Zhang Guangfan, et al., Active health monitoring of an aircraft wing with embedded piezoelectric sensor/actuator network: I. Defect detection, localization and growth monitoring[J], Smart Mater. Struct. 16 (4) (2007) 1208–1217.
[22] Wang Dong, Lu.Yu. Ye Lin, A probabilistic diagnostic algorithm for identification of multiple notches using digital damage fingerprints (DDFs) [J], J. Intell. Mater. Syst. Struct. 20 (12) (2009) 1439–1450.
[23] Wu. Zhanjun, Liu Kehai, Wang Yishou, et al., Validation and evaluation of damage identification using probability-based diagnostic imaging on a stiffened composite panel[J], J. Intell. Mater. Syst. Struct. 26 (16) (2014) 2181–2195.
[24] Tang Ziqiao, Abera Gezaei, M.B. Kishore, et al., An applicable time reversal analysis of guided waves in Al-plate with ultrasonic immersion testing [J], J. Korean Phys. Soc. 74 (4) (2019) 340–348.
[25] Huang Liping, Zeng Liang, Lin Jing, et al., An improved time reversal method for diagnostics of composite plates using Lamb waves [J], Compos. Struct. 190 (2018) 10–19.
[26] Hu.a. Jiadong, Lin Jing, Zeng Liang, High-resolution damage detection based on local signal difference coefficient model[J], Struct. Health Monit. 14 (1) (2015) 20–34.
[27] H. Park, H. Sohn, K.H. Law, Damage detection in composite plates by using an enhanced time reversal method [J], J. Aerosp. Eng. 20 (3) (2007) 141–151.